Nano Research

ISSN 1998-0124 CN 11-5974/O4
https://doi.org/10.1007/s12274-020-2756-2

Research Article

Confining ultrafine Li_3P nanoclusters in porous carbon for high-performance lithium-ion battery anode

Eryang Mao[1], Wenyu Wang[1] Mintao Wan[1], Li Wang[2] (✉), Xiangming He[2], and Yongming Sun[1] (✉)

[1] *Wuhan National Laboratory for Optoelectronics, Huazhong University of Science and Technology, Wuhan 430074, China*
[2] *Institute of Nuclear and New Energy Technology, Tsinghua University, Beijing 100084, China*

Received: 4 December 2019 / **Revised:** 11 February 2020 / **Accepted:** 12 March 2020

ABSTRACT

High-capacity lithium-containing alloy anodes (e.g., $Li_{4.4}Si$, $Li_{4.4}Sn$, and Li_3P) enable lithium-free cathodes (e.g., Sulfur, V_2O_5, and FeF_3) to produce next-generation lithium-ion batteries (LIBs) with high energy density. Herein, we design a Li_3P/C nanocomposite with Li_3P ultrafine nanodomains embedded in micrometer-scale porous carbon particles. Benefiting from the unique micro/nanostructure of the Li_3P/C nanocomposite, electrons transfer rapidly through the conductive pathway provided by the porous carbon framework and the volume change between Li_3P and P is confined in the nanopores of the carbon, which avoids the collapse of the whole Li_3P/C composite particles. As expected, the as-achieved Li_3P/C nanocomposite provided a high available lithium-ion capacity of 791 mAh/g (calculated based on the mass of Li_3P/C) at 0.1 C during the initial delithiation process. Meanwhile, the Li_3P/C nanocomposite showed 75% of its 0.5 C capacity at 6 C and stable cycling stability.

KEYWORDS

Li_3P nanoclusters, porous carbon, lithium-containing anode, high capacity, lithium-ion batteries

1 Introduction

Rechargeable lithium-ion batteries (LIBs) are boosting a flourishing era of portable electronic devices and zero-emission electric vehicles and they also exhibit great potential for the storage of renewable energy, such as solar, geothermal, water, tidal and wind power [1–4]. With the prosperity of these applications, more and more novel technologies and innovative mechanisms have been put forward to achieve higher energy density, longer cycle life, higher rate performance, and better safety beyond the commercially available LIBs [5–7]. In the existing LIBs, intercalated lithium oxide or phosphate cathodes provide lithium ions for battery cycling. Although great improvement has been achieved in the electrochemical performance of intercalated cathode materials [8–10], further advancement in energy density of batteries is hindered by their limited specific capacities (typically < 200 mAh/g). Alternatively, lithium-free cathode materials typically deliver much higher theoretical capacities than intercalated lithium oxide materials, such as 1,672 mAh/g for sulfur [11], 441 mAh/g for V_2O_5 [12] and 712 mAh/g for FeF_3 [13]. Thus, much higher energy density can be expected for LIBs using these lithium-free cathode materials, once they are successfully paired with high-capacity lithium-containing anode materials.

Due to its highest theoretical capacity (3,860 mAh/g, 2,061 mAh/cm^3), lithium metal is the ultimate lithium-containing anode and is experiencing a time of revival in recent years [14–17]. However, the problems of uncontrolled dendritic lithium formation and its high chemical reactivity cause serious safety concerns and low Coulombic efficiency (typically < 95% in commercial carbonate electrolytes), making lithium metal anode still far from real applications [18, 19]. By replacing the lithium-deposition/stripping mechanism with alloying/dealloying mechanism, alloy anodes (e.g., Si, Sn and Al) avoid the problems of lithium dendrite formation and exhibit higher Coulombic efficiency than lithium metal while still delivering high theoretical specific capacities (e.g., 2011 mAh/g for Si, 994 mAh/g for Sn, and 2235 mAh/g for Al). Thus, lithium alloys are promising lithium-containing anode materials for next-generation LIBs with high energy density [20–23]. Recently, Li_xSi_y/graphene hybrid has been investigated as an attractive lithium-containing anode material that provides high lithium-ion capacity and good cycling stability [24], which paves the way to the new battery chemistry using lithium-free cathode materials.

Red P is abundant, low-cost and stable in air [25]. It reacts electrochemically with lithium to form Li_3P ($P + 3Li^+ + 3e^- \rightarrow Li_3P$) and delivers a high theoretical capacity (2,596 mAh/g, 6,075 mAh/cm^3) and reasonable lithiation potential (~ 0.7 V in average vs. Li+/Li) [26–29]. The high capacity of red P enables high energy density of batteries, and its safe lithiation potential with reasonable potential gap between lithium metal and red P [30, 31] avoids lithium metal plating at high current densities or at low temperatures [32]. In comparison to P, Li_3P, the fully lithiated state of P, represents a more attractive anode material, since it circumvents the volumetric expansion problem in P anode due to its fully expanded state, and it can be compatible with high-capacity lithium-free cathodes to achieve high energy density of full batteries. Despite these advantages, Li_3P is plagued with three main challenges: (i) the insulating nature of Li_3P leads to sluggish solid-state diffusion processes; (ii) the large volume change of Li_3P during cycling causes the continual breakage and formation of solid-electrolyte interphase

Address correspondence to Yongming Sun, yongmingsun@hust.edu.cn; Li Wang, wang-l@tsinghua.edu.cn

(SEI), and eventually exhaustion of the electrolyte; (iii) the moisture sensitivity of Li_3P makes it unstable in the environment of materials synthesis and battery fabrication. Close attention should be paid to improving the conductivity and stability of Li_3P to achieve high electrochemical performance of Li_3P based electrodes. Till now, successful examples of Li_3P-based anodes for LIBs has not yet been reported.

Material structural design toward high conductivity and high active material utilization is of vital importance to achieve good electrochemical performance of battery materials. So far, incorporating active nanomaterials within an electrically conductive porous carbon matrix or other carbon-based composite is considered as one of the most effective strategies to address the existing challenges of insulating electrode materials and improve their electrochemical performance [15, 33]. Here, we report a Li_3P/C nanostructure, consisting of an electrochemically active Li_3P nanodomains embedded in a porous carbon matrix with particle size of several micrometers, delivers high capacity, good rate capability and stable cycle life. As illustrated in Fig. 1, such structure has multiple advantages: (i) an interconnected porous carbon network enables rapid electron transport, (ii) small size of Li_3P nanoparticles with a short solid-phase ion diffusion length leads to fast solid-phase reaction and high utilization of active materials, and (iii) Li_3P/C embedded structure confines the volume change during charge/discharge within the nanopores of the carbon particles and thus avoid the collapse of the overall composite particle and electrode structure, leading to the formation of a stable SEI layer during cycling.

2 Experimental

2.1 Synthesis of Li_3P/C nanocomposite

The red P/C nanocomposite was firstly prepared according to our previous work via a sublimation and adsorption approach using red P power and porous carbon as the starting materials [28, 34]. The red P/C composite was mixed with molten lithium and they reacted under continuous mechanical stirring at 200 °C for 1 h to produce Li_3P/C nanocomposite in an Argon-filled glove box with moisture level below 0.1 ppm and oxygen level below 0.2 ppm.

2.2 Materials characterization

Scanning electron microscopy (SEM) was performed on FEI Nova NanoSEM 450 device. Powder X-ray diffraction (XRD) patterns of Li_3P/C nanocomposite were collected on a PANalytical B.V., Holland with Cu Kα radiation (λ = 0.154 nm). The XRD samples were sealed with Kapton tape (DuPont) to eliminate possible side reactions in the air. Transmission electron microscopy (TEM) and high-resolution TEM (HRTEM) were taken on a FEI Titan 80–300 environmental TEM at an acceleration voltage of 300 kV. Nitrogen adsorption measurements were achieved on V-Sorb 2,800 at 77 K. Thermogravimetric analysis (TGA) was performed under dry air atmosphere at a heating rate of 5 °C/min from room temperature to 1,200 °C.

2.3 Electrochemical measurements

To investigate the electrochemical performances of Li_3P/C anode, Coin cells of type-2032 were assembled using a commercial Li metal foil as counter/reference electrode with 120 μL carbonate-based electrolyte (1M $LiPF_6$ in EC/DEC (v/v = 1/1)). To prepare the Li_3P/C electrodes, Li_3P/C composites, carbon black (Super P, TIMCAL, Switzerland), and polyvinylidenefluoride binder (PVDF, Kynar HSV 900) (70:20:10 by weight) were dispersed uniformly in THF (Sigma Aldrich) to form a slurry. The slurry was then drop casted onto a copper foil and dried in an Ar-filled glove box. The total mass loading of Li_3P/C anode was ~ 1 mg/cm^2. Galvanostatic cycling of Li_3P/C cells was carried out on a Landt battery tester. The current density during the battery test for 1 C was 2,596 mAh/g based on P (or 1,552 mAh/g based on Li_3P).

3 Results and discussion

The as-achieved red P/C nanocomposite featured nanoscale red P nanodomains confined in micrometer-scale nanoporous carbon particles with internal nanoscale void space (Fig. S1 in the Electronic Supplementary Material (ESM)). The red P/C powder then was mixed with molten lithium in argon atmosphere at 200 °C under mechanical stirring. Due to the high reactivity between red P and lithium, the amorphous red P nanodomains gradually turned into Li_3P nanoparticles ($P + 3Li \rightarrow Li_3P$) that embedded in the nanopores of the carbon particles. Despite of the volume expansion from red P to Li_3P, the lithiation of red P would not cause large volume change at the entire composite particle level due to the existence of internal nanoscale void pace.

Figures 2(a) and 2(b) show the scanning electron microscopy (SEM) images of the porous carbon and as-achieved Li_3P/C nanocomposite. It is observed that the porous carbon and Li_3P/C nanocomposite particles show similar morphology with irregular shapes and a wide size distribution mainly from 5 to 10 μm, indicating that the lithiation process of red P does not cause the pulverization of the composite particles. Moreover, there is no Li_3P individual particle observed in the Li_3P/C nanocomposite (Fig. 2(c) and Fig. S2 in the ESM), suggesting that the Li_3P is mainly embedded inside the porous carbon particles. The crystallinity and phase of the Li_3P/C nanocomposite were measured by XRD. As displayed in Fig. 2(d), broad peaks with reduced intensity for Li_3P were observed in the XRD pattern, which indicated the existence of Li_3P nanoparticles. The bare carbon and product after reaction between the porous carbon and molten lithium showed very similar XRD patterns (Fig. S3 in the ESM), and the carbon in the Li_3P/C contributed very limited reversible capacity (~ 0.8 mAh/g, Fig. S4 in the ESM) in comparison to the overall capacity of the nanocomposite. The Li_3P is the main active material and the carbon functions

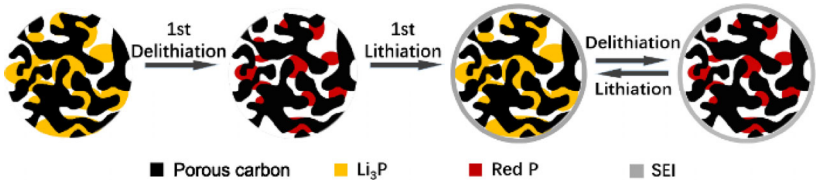

Figure 1 Schematic of Li_3P/C nanocomposite for high-capacity lithium-containing battery anode. Li_3P nanoclusters are embedded in the nanopores of the carbon particles. The interconnected carbon framework of the porous carbon works as the conductive skeleton for fast electron transport. The ultrafine particle size of Li_3P enables fast electrochemical reactions. The volume change of Li_3P/P active material is confined within the nanopores of the carbon particles and stable SEI layer is formed at the outer surface of the Li_3P/C composite particle during cycling.

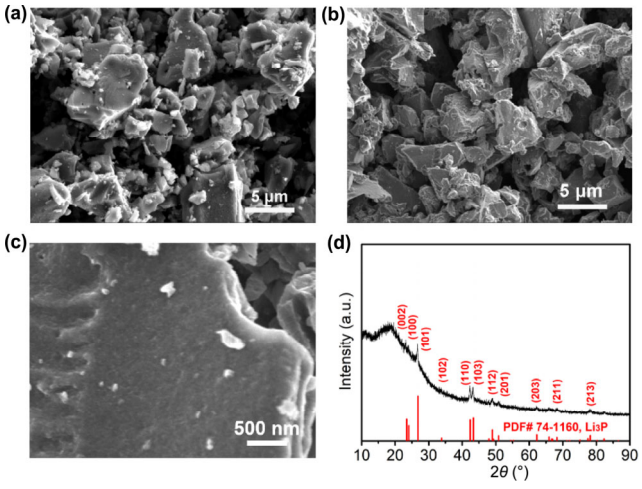

Figure 2 SEM images of (a) the porous carbon and (b) the Li_3P/C nanocomposite, (c) high-resolution SEM image and (d) XRD pattern of the Li_3P/C nanocomposite. The porous carbon and Li_3P/C nanocomposite particles exhibited irregular shapes and similar size distribution and Li_3P individual particles were not observed in the Li_3P/C nanocomposite, suggesting the successful implantation of Li_3P into the pores of the carbon. Broad peaks with reduced intensity for Li_3P were observed in the XRD pattern of Li_3P/C nanocomposite, indicating the existence of Li_3P nanoparticles.

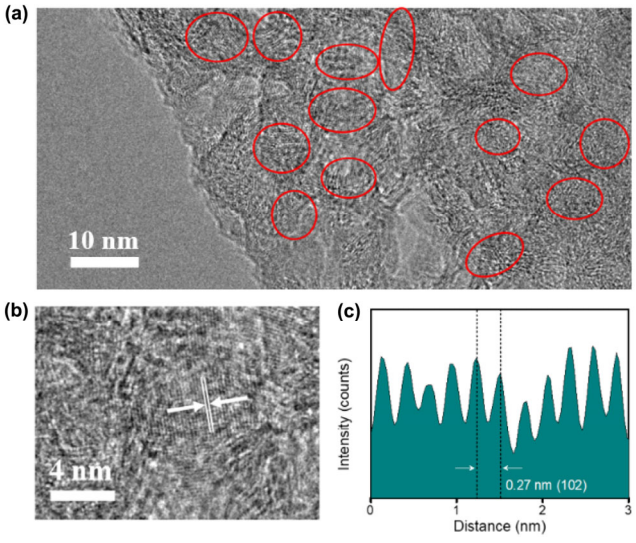

Figure 3 (a) TEM image of the Li_3P/C nanocomposite, showing that Li_3P nanodomains are uniformly distributed in the porous carbon matrix. (b) HRTEM image and (c) the corresponding fringes of a Li_3P nanodomain, indicating its crystallinity and small domain size. Close contact between the Li_3P nanodomain and the carbon matrix was observed, leading to good electronic conductivity.

mainly as the matrix. Thus, Li_3P/C is used to describe the as-prepared composite structure.

The microstructure of the Li_3P/C nanocomposite was further examined by TEM. Figure 3(a) shows a representative bright-field TEM image of the Li_3P/C nanocomposite. Li_3P domains labelled by circles were randomly distributed in an amorphous carbonaceous matrix. The size of the Li_3P domains ranges from 10 to 15 nm. The crystallinity of Li_3P was confirmed by HRTEM (Figs. 3(b) and 3(c)). The interplanar spacing of ~ 0.27 nm corresponds to (102) lattice planes of hexagonal Li_3P. In contrast to the abundant nanopores of existing in initial porous carbon particles (Fig. S5 in the ESM), much less nanopores were observed for the Li_3P/C nanocomposite under TEM, suggesting the successful embedment of Li_3P nanoparticles in the porous carbon. Due to the embedment of Li_3P into the porous carbon, dark/light contrast was clearly observed for the Li_3P/C nanocomposite (Fig. 3(a)). The Brunauer–Emmett–Teller (BET) surface area of the Li_3P/C nanocomposite was significantly reduced after the embedment of Li_3P nanodomains into the porous carbon from 1,362.42 m^2/g for the pristine porous carbon to 5.43 m^2/g for the Li_3P/C nanocomposite (Fig. S6 in the ESM). This result indicated that most of the pores of the carbon were filled with Li_3P, well consistent with the TEM investigation. The carbon content in the Li_3P/C nanocomposite is 40.1% according to the TG result (Fig. S7 in the ESM). Due to the advantages of the embedded structure of Li_3P/C nanocomposite, stable battery cycling and high capacity of the Li_3P anode material can be expected. During the delithiation and lithiation processes, the volume change of Li_3P/P nanodomains can be confined in the nanopores of the carbon. The carbonaceous matrix can work as the conductive path for electron transport within the Li_3P/C composite particles, providing high electron conductivity.

The electrochemical lithium storage property of the as-achieved Li_3P/C nanocomposite was characterized in coin cells with the constant current–voltage technique. The Li_3P/C electrode was evaluated with a lithium metal half-cell configuration at low current density of 0.1 C for the first cycle to measure the amount of the pre-stored active lithium in the Li_3P/C composite. As shown in Fig. S8 in the ESM, the Li_3P/C electrode exhibited a high first-cycle delithiation capacity of 791 mAh/g (calculated based on the mass of Li_3P/C) with the delithiation voltage of ~ 1.04 V in average, showing that most of the P in the starting material was successfully converted into electrochemical active Li_3P during the synthesis of the Li_3P/C nanocomposite. During the first-cycle lithiation process, a high lithiation capacity of 776 mAh/g was achieved for the Li_3P/C composite, and the average voltage was ~ 0.68 V during the lithiation process. With the lithiation capacity very close to the delithiation capacity, the Coulombic efficiency was 102% for the first cycle, indicating the complete lithiation of P and carbon during the fabrication process of Li_3P/C nanocomposite and high reversibility of the Li_3P/C electrode. To void the confusion of terminology in the following discussion, here we define the charge as the lithiation for the P/C electrode, since it undergoes the lithiation process during the charge process of a full lithium-ion battery. P-based anode is promising for fast-charging lithium-ion batteries due to its high capacity and relatively low, yet safe, lithiation potential [34]. To measure the fast-charging capacity of the as-achieved Li_3P/C nanocomposite, electrochemical cycling at various C rates with a constant delithiation current of 0.2 C were performed (Figs. 4(a) and 4(b)). At 0.5 C, the lithiation capacity of the Li_3P/C electrode was 620 mAh/g. 82% and 75% of the capacity at 0.5 C were maintained for the Li_3P/C electrode at 4 and 6 C, exhibiting good fast-charging capability of the Li_3P/C nanocomposite as an anode material. The average lithiation voltage of the electrode was 0.39 V (vs. Li^+/Li) at 6 C, which is safe enough to avoid the lithium plating during the fast-charging. Importantly, the capacity recovers to 617 mAh/g after the rate measurement. Long-term stability of the Li_3P/C electrode was further tested at 0.2 C (Figs. 4(a) and 4(c)). The Li_3P/C nanocomposite delivered a high reversible capacity of 626 mAh/g at the 101st cycle. At the 200th cycle, the capacity of the Li_3P/C nanocomposite still reached 580 mAh/g, exhibiting good cycling stability due to the unique structure with active Li_3P nanodomains confined in the porous micrometer-scale carbon particles.

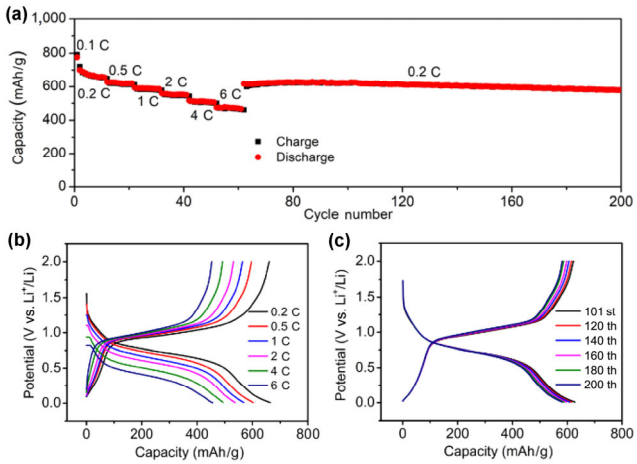

Figure 4 (a) Cycling of the Li_3P/C electrode cycled at various lithiation current densities with a constant delithiation current density of 0.2 C and ((b) and (c)) the corresponding voltage–capacity plots. The galvanostatic charge/discharge measurement for $Li_3P/C||Li$ metal cells was carried out with the cut-off potential range of 0.01–2 V.

The stability test of this composite to ambient air was performed. XRD measurement was conducted for the Li_3P/C nanocomposite before and after exposure to ambient air. As shown in Fig. S9 in the ESM, XRD peaks for Li_3P were observed for the Li_3P/C nanocomposite after resting in ambient air for 6 h, indicating that Li_3P phase in the Li_3P/C nanocomposite was mainly maintained. The first-cycle delithiation capacities of the Li_3P/C electrodes were investigated after their exposure to ambient air for different time (0, 3 and 6 h, Fig. S10 in the ESM). The first-cycle delithiation capacity for the measured fresh Li_3P/C electrode was 752 mAh/g calculated based on the mass of Li_3P/C at 0.1 C. The capacity degraded with the increase of time exposed to ambient air. After exposure for 3 and 6 h, the first-cycle delithiation capacities of Li_3P/C electrodes were 608 and 389 mAh/g, with the corresponding capacity retention of 80.9% and 52.0%, respectively. These results indicate that the composite structure of Li_3P/C improves the ambient stability of Li_3P.

4 Conclusion

When the Li_3P/C composite reported here is compared with other battery anode materials (e.g., Si and Al), it is clear that we have been able to achieve a unique combination of high pre-stored lithium-ion capacity, good fast-charging capability and stable cycling stability, which has not been reported before. This advance is a result of the unique structure design which incorporates active Li_3P ultrafine nanoparticles into porous conductive carbon host with micrometer scale, improve the conductivity of the active material and confine the volume change of the active material within the pores of the carbon host. In the future, the high-capacity Li_3P/C composite can be paired with high-capacity lithium-free battery cathode (such as S and V_2O_5) to construct next-generation high-energy-density lithium-ion batteries. Also, the high-capacity Li_3P/C composite can also work as a prelithition additive to address the initial lithium loss in lithium-ion batteries.

Acknowledgements

This work was supported by the National Natural Science Foundation of China (No. 51802105) and Innovation Fund of Wuhan National Laboratory for Optoelectronics. E. M. acknowledges support from the Fundamental Research Funds for the Central Universities (HUST: 2019JYCXJJ014). The authors would like to thank the Analytical and Testing Center of Huazhong University of Science and Technology as well as the Center for Nanoscale Characterization & Devices of Wuhan National Laboratory for Optoelectronics for providing the facilities to conduct the characterization.

Electronic Supplementary Material: Supplementary material (experimental details and additional characterizations) is available in the online version of this article at https://doi.org/10.1007/s12274-020-2756-2.

References

[1] Lu, J.; Chen, Z. W.; Pan, F.; Cui, Y.; Amine, K. High-performance anode materials for rechargeable lithium-ion batteries. *Electrochem. Energy Rev.* **2018**, *1*, 35–53.
[2] Chu, S.; Cui, Y.; Liu, N. The path towards sustainable energy. *Nat. Mater.* **2017**, *16*, 16–22.
[3] Dunn, B.; Kamath, H.; Tarascon, J. M. Electrical energy storage for the grid: A battery of choices. *Science* **2011**, *334*, 928–935.
[4] Armand, M.; Tarascon, J. M. Building better batteries. *Nature* **2008**, *451*, 652–657.
[5] Manthiram, A. An outlook on lithium ion battery technology. *ACS Central Sci.* **2017**, *3*, 1063–1069.
[6] Choi, J. W.; Aurbach, D. Promise and reality of post-lithium-ion batteries with high energy densities. *Nat. Rev. Mater.* **2016**, *1*, 16013.
[7] Whittingham, M. S. Ultimate limits to intercalation reactions for lithium batteries. *Chem. Rev.* **2014**, *114*, 11414–11443.
[8] Yan, P. F.; Zheng, J. M.; Liu, J.; Wang, B. Q.; Cheng, X. P.; Zhang, Y. F.; Sun, X. L.; Wang, C. M.; Zhang, J. G. Tailoring grain boundary structures and chemistry of Ni-rich layered cathodes for enhanced cycle stability of lithium-ion batteries. *Nat. Energy* **2018**, *3*, 600–605.
[9] Liu, Q.; Su, X.; Lei, D.; Qin, Y.; Wen, J. G.; Guo, F. M.; Wu, Y. A.; Rong, Y. C.; Kou, R. H.; Xiao, X. H. et al. Approaching the capacity limit of lithium cobalt oxide in lithium ion batteries via lanthanum and aluminium doping. *Nat. Energy* **2018**, *3*, 936–943.
[10] Sander, J. S.; Erb, R. M.; Li, L.; Gurijala, A.; Chiang, Y. M. High-performance battery electrodes via magnetic templating. *Nat. Energy* **2016**, *1*, 16099.
[11] Ji, X. L.; Lee, K. T.; Nazar, L. F. A highly ordered nanostructured carbon-sulphur cathode for lithium-sulphur batteries. *Nat. Mater.* **2009**, *8*, 500–506.
[12] Chen, X. Y.; Zhu, H. L.; Chen, Y. C.; Shang, Y. Y.; Cao, A. Y.; Hu, L. B.; Rubloff, G. W. Mwcnt/V_2O_5 core/shell sponge for high areal capacity and power density Li-ion cathodes. *ACS Nano* **2012**, *6*, 7948–7955.
[13] Li, H.; Balaya, P.; Maier, J. Li-storage via heterogeneous reaction in selected binary metal fluorides and oxides. *J. Electrochem. Soc.* **2004**, *151*, A1878.
[14] Cheng, X. B.; Zhang, R.; Zhao, C. Z.; Zhang, Q. Toward safe lithium metal anode in rechargeable batteries: A review. *Chem. Rev.* **2017**, *117*, 10403–10473.
[15] Sun, Y. M.; Liu, N.; Cui, Y. Promises and challenges of nanomaterials for lithium-based rechargeable batteries. *Nat. Energy* **2016**, *1*, 16071.
[16] Zheng, G. Y.; Lee, S. W.; Liang, Z.; Lee, H. W.; Yan, K.; Yao, H. B.; Wang, H. T.; Li, W. Y.; Chu, S.; Cui, Y. Interconnected hollow carbon nanospheres for stable lithium metal anodes. *Nat. Nanotechnol.* **2014**, *9*, 618–623.
[17] Liu, J.; Bao, Z.; Cui, Y.; Dufek, E. J.; Goodenough, J. B.; Khalifah, P.; Li, Q. Y.; Liaw, B. Y.; Liu, P.; Manthiram, A. et al. Pathways for practical high-energy long-cycling lithium metal batteries. *Nat. Energy* **2019**, *4*, 180–186.
[18] Lin, D. C.; Liu, Y. Y.; Cui, Y. Reviving the lithium metal anode for high-energy batteries. *Nat. Nanotechnol.* **2017**, *12*, 194–206.
[19] Albertus, P.; Babinec, S.; Litzelman, S.; Newman, A. Status and challenges in enabling the lithium metal electrode for high-energy and low-cost rechargeable batteries. *Nat. Energy* **2018**, *3*, 16–21.
[20] Wang, C.; Yu, J. M.; Li, S. H.; Lu, Z. D. Boosting the cycling stability of Li Si alloy microparticles through electroless copper deposition. *Chem. Eng. J.* **2019**, *370*, 1019–1026.

[21] Jiang, M. W.; Yu, Y.; Fan, H. M.; Xu, H.; Zheng, Y. H.; Huang, Y. H.; Li, S.; Li, J. Full-cell cycling of a self-supporting aluminum foil anode with a phosphate conversion coating. *ACS Appl. Mater. Interfaces* **2019**, *11*, 15656–15661.

[22] Xu, H.; Li, S.; Chen, X. L.; Zhang, C.; Liu, W. J.; Fan, H. M.; Yu, Y.; Huang, Y. H.; Li, J. Sn-alloy foil electrode with mechanical prelithiation: Full-cell performance up to 200 cycles. *Adv. Energy Mater.* **2019**, *9*, 1902150.

[23] Xu, H.; Li, S.; Zhang, C.; Chen, X. L.; Liu, W. J.; Zheng, Y. H.; Xie, Y.; Huang, Y. H.; Li, J. Roll-to-roll prelithiation of Sn foil anode suppresses gassing and enables stable full-cell cycling of lithium ion batteries. *Energy Environ. Sci.* **2019**, *12*, 2991–3000.

[24] Zhao, J.; Zhou, G. M.; Yan, K.; Xie, J.; Li, Y. Z.; Liao, L.; Jin, Y.; Liu, K.; Hsu, P. C.; Wang, J. Y. et al. Air-stable and freestanding lithium alloy/graphene foil as an alternative to lithium metal anodes. *Nat. Nanotechnol.* **2017**, *12*, 993–999.

[25] Corbridge, D. E. C. *Phosphorus: Chemistry*, *Biochemistry and Technology*; 6th ed. CRC Press: Boca Raton, FL, 2013.

[26] Sun, J.; Zheng, G. Y.; Lee, H. W.; Liu, N.; Wang, H. T.; Yao, H. B.; Yang, W. S.; Cui, Y. Formation of stable phosphorus–carbon bond for enhanced performance in black phosphorus nanoparticle-graphite composite battery anodes. *Nano Lett.* **2014**, *14*, 4573–4580.

[27] Qian, J. F.; Qiao, D.; Ai, X. P.; Cao, Y. L.; Yang, H. X. Reversible 3-Li storage reactions of amorphous phosphorus as high capacity and cycling-stable anodes for Li-ion batteries. *Chem. Commun.* **2012**, *48*, 8931–8933.

[28] Wang, L.; He, X. M.; Li, J. J.; Sun, W. T.; Gao, J.; Guo, J. W.; Jiang, C. Y. Nano-structured phosphorus composite as high-capacity anode materials for lithium batteries. *Angew. Chem., Int. Ed.* **2012**, *51*, 9034–9037.

[29] Li, W. H.; Yang, Z. Z.; Li, M. S.; Jiang, Y.; Wei, X.; Zhong, X. W.; Gu, L.; Yu, Y. Amorphous red phosphorus embedded in highly ordered mesoporous carbon with superior lithium and sodium storage capacity. *Nano Lett.* **2016**, *16*, 1546–1553.

[30] Chan, C. K.; Peng, H. L.; Liu, G.; McIlwrath, K.; Zhang, X. F.; Huggins, R. A.; Cui, Y. High-performance lithium battery anodes using silicon nanowires. *Nat. Nanotechnol.* **2008**, *3*, 31–35.

[31] Ohzuku, T.; Iwakoshi, Y.; Sawai, K. Formation of lithium-graphite intercalation compounds in nonaqueous electrolytes and their application as a negative electrode for a lithium ion (shuttlecock) cell. *J. Electrochem. Soc.* **1993**, *140*, 2490–2498.

[32] Liu, Q. Q.; Du, C. Y.; Shen, B.; Zuo, P. J.; Cheng, X. Q.; Ma, Y. L.; Yin, G. P.; Gao, Y. Z. Understanding undesirable anode lithium plating issues in lithium-ion batteries. *RSC Adv.* **2016**, *6*, 88683–88700.

[33] Li, W.; Liu, J.; Zhao, D. Y. Mesoporous materials for energy conversion and storage devices. *Nat. Rev. Mater.* **2016**, *1*, 16023.

[34] Sun, Y. M.; Wang, L.; Li, Y. B.; Li, Y. Z.; Lee, H. R.; Pei, A.; He, X. M.; Cui, Y. Design of red phosphorus nanostructured electrode for fast-charging lithium-ion batteries with high energy density. *Joule* **2019**, *3*, 1080–1093.